NÖHÜ Müh. Bilim. Derg. / NOHU J. Eng. Sci., 2022; 11(1), 157-169

Niğde Ömer Halisdemir Üniversitesi Mühendislik Bilimleri Dergisi
Niğde Ömer Halisdemir University Journal of Engineering Sciences

Araştırma makalesi / Research article

www.dergipark.org.tr/tr/pub/ngumuh / www.dergipark.org.tr/en/pub/ngumuh

Geochemistry of Upper Eocene-Oligocene sandstones from Tuzgölü Basin (Central Anatolia)

Tuzgölü Havzasından Üst Eosen-Oligosen kumtaşlarının jeokimyası (Orta Anadolu)

Mehmet Yavuz Hüseyinca [1,*], Şuayip Küpeli [2]

[1,2] *Konya Technical University, Geological Engineering Department, 42250, Konya, Turkey*

Abstract

In this study, mineralogical and geochemical features of Upper Eocene-Oligocene sandstones exposed by the Tuzgölü Fault Zone (TFZ) at the eastern border of the Tuzgölü Basin were investigated. The absence of zircon enrichment in the Zr/Sc-Th/Sc diagram indicated no sedimentary recycling. This shows that the sandstones are first cycle sediments, that is, the material transported directly from the source. Critical element ratios for provenance such as La/Sc, La/Co, Th/Sc, Th/Co, Th/Cr, Zr/Sc, Zr/Co, Ba/Sc, and Ba/Co, Th/Sc-Eu/Eu* diagram and average Rare Earth Element (REE) pattern suggest a provenance in "intermediate magmatic" composition. The variation in the negative Ce anomaly effect observed between the lower and upper parts of the sequence indicates variation in the oxygen level of the water. In each of the La-Th-Sc, Th-Co-Zr/10, and Th-Sc-Zr/10 tectonic setting discrimination diagrams, the sandstone average fell onto the "Continental Island Arc" position. This tectonic setting defines the arc that developed along the continental margin of the subduction zone. The tectonic setting found for the basin, supported the evolution model that the Tuzgölü Basin developed as a fore-arc basin.

Keywords: Ce anomaly, Provenance, Sandstone, Tectonic setting, Tuzgölü Basin

Özet

Bu çalışmada, Tuzgölü Havzasının doğu sınırında Tuzgölü Fay Zonu (TFZ) tarafından açığa çıkarılmış olan Üst Eosen-Oligosen kumtaşlarının mineralojik ve jeokimyasal özellikleri incelenmiştir. Th/Sc-Zr/Sc diyagramında zirkon zenginleşmesinin olmaması, sedimanter tekrardan çevrim olmadığını belirtmiştir. Bu, kumtaşlarının birinci döngü çökel olduğunu yani malzemenin doğrudan kaynaktan gelmiş olduğunu göstermektedir. La/Sc, La/Co, Th/Sc, Th/Co, Th/Cr, Zr/Sc, Zr/Co, Ba/Sc ve Ba/Co gibi provenans için kritik element oranları, Th/Sc-Eu/Eu* diyagramı ve ortalama Nadir Toprak Element (NTE) deseni, "ortaç magmatik" bileşimli bir provenansı önermektedir. İstifin alt ve üst kısımları arasında gözlemlenen negatif Ce anomalisi etkisindeki farklılık, suyun oksijen seviyesinde değişim olduğunu göstermektedir. La-Th-Sc, Th-Co-Zr/10 ve Th-Sc-Zr/10 tektonik konum ayırma diyagramlarının her birinde kumtaşı ortalaması "Kıtasal Adayayı" konumuna düşmüştür. Bu tektonik konum dalma batma zonunun kıta kenarında gelişen bir yaydır. Bulunan tektonik konum, Tuzgölü Havzasının bir yay önü havza olarak geliştiği yönündeki evrim modelini desteklemiştir.

Anahtar kelimeler: Ce anomalisi, Kumtaşı, Provenans, Tektonik konum, Tuzgölü Havzası

1 Introduction

Tuzgölü Basin is located in the central part of Anatolia (Figure 1). The basin has been the subject of many studies due to its geology, hydrocarbon potential and evaporite-bearing sediments [1-11].

There are two different views in the literature regarding the tectonic evolution of the basin. One of them suggests that the basin developed as a fore-arc basin together with the Haymana Basin [12, 13]. The other suggests that the basin developed in the intra-continental rifting zone [14, 15]. In this study, Upper Eocene-Oligocene sandstones exposed by the TFZ at the eastern border of the basin were investigated. Clastic sediments can keep geochemical records of the effects they have been exposed to, from the source to the diagenesis. Therefore, geochemical records are very useful for determining provenance and tectonic setting. This paper aimed to contribute to the discussion in the literature by making inferences about the tectonic setting of the source region in the period when the sandstones were deposited, as well as providing an understanding of the geochemistry of the sandstones.

1.1 Regional tectonic setting

The opening and closing movements of the oceans in the Tethyan region caused many continental blocks to break away from the main continents. Therefore, the collision boundary between Laurasia and Gondwana can't be represented by a single suture line [16]. This situation is very evident in Anatolia, which is an important component of the Alp-Himalayan orogenic belt. The Anatolian landmass consists of several micro-continents that were aggregated

* Sorumlu yazar / Corresponding author, e-posta / e-mail: myhuseyinca@ktun.edu.tr (M. Y. Hüseyinca)
Geliş / Recieved: 03.11.2021 Kabul / Accepted: 27.12.2021 Yayımlanma / Published: 14.01.2022
doi: 10.28948/ngmuh.1018818

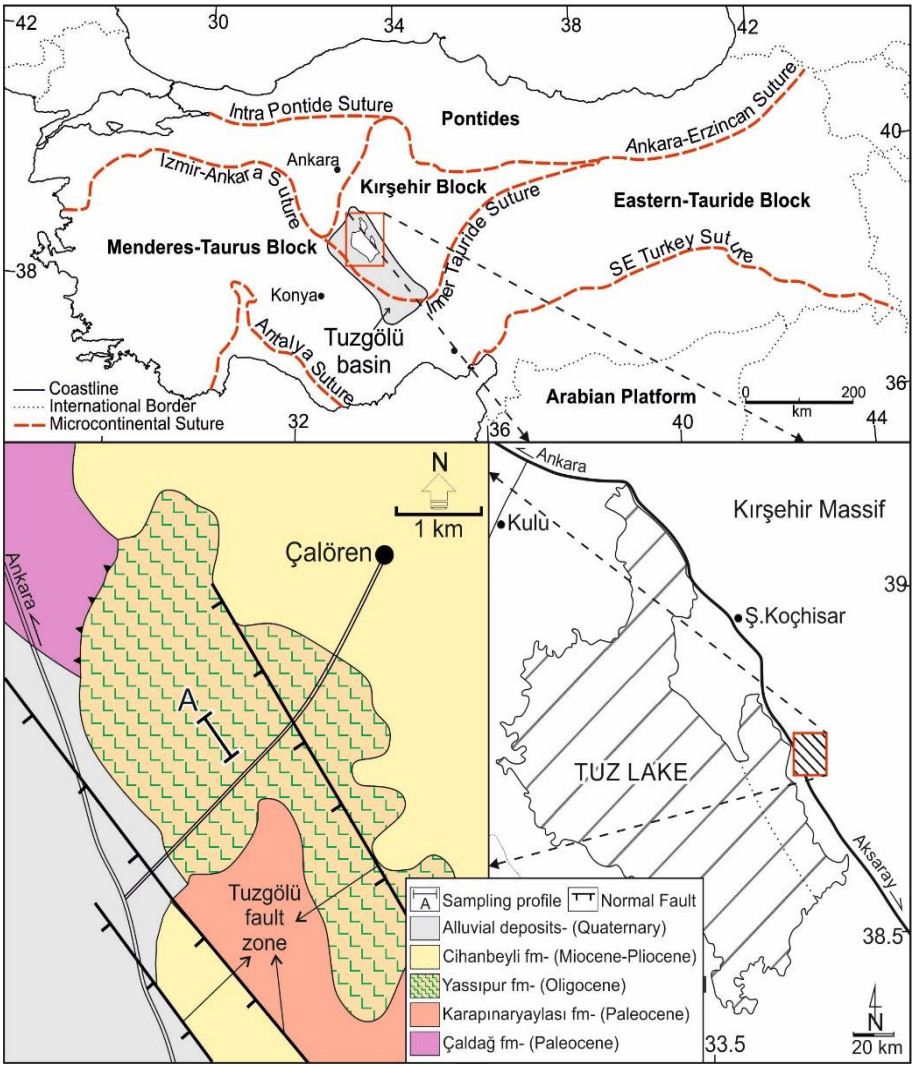

Figure 1. Major terrane divisions of Turkey with associated sutures [16] and detailed geological map of the study area [23].

due to the closure of different branches of the Tethyan Ocean [17-21] (Figure 1). During the Neo-Tethyan evolution of Turkey, several sedimentary basins called the Central Anatolian Basins formed between these micro-continents [22]. Tuzgölü Basin is one of these inner basins.

1.2 Tuzgölü Basin deposits

The basin is bordered by the Kırşehir Massif in the east [24], the Kütahya-Bolkardağı belt in the west and south [25], and the Samsam heights in the north [26]. A thick sedimentary succession was deposited in the basin between Late Cretaceous and Quaternary (Figure 2). Deep drillings, geophysical surveys, outcrops exposed by the TFZ and correlation with the adjacent Haymana Basin are the main sources of sedimentary data on this succession. The main reason for this is that the basin fill was mostly covered by younger sediments. The TFZ is a normal fault system, with a right-lateral strike-slip and sometimes a small reverse component [27, 28].

The basin fill deposited until the Upper Eocene is mainly represented by redbeds and conglomerates (Kartal Formation), thick turbidites (Karapınaryaylası Formation), and local limestones (Asmaboğazı Member and Çaldağ Formation). Upper Eocene-Oligocene sediments consisting of shallow marine-terrestrial clastics and evaporites (Yassıpur Formation) unconformably overlie these older units. Miocene sediments are represented by the coal-bearing lake deposits (Koçhisar Formation) that unconformably overlie the previous units. The Mio-Pliocene sediments including conglomerate, sandstone, siltstone, claystone, and lacustrine limestones (Cihanbeyli Formation) overlie the previous formations. Quaternary alluvial deposits mostly cover all the older units (Figure 2).

The sandstones investigated in this study are found in the upper part of the Yassıpur Formation (Figure 3). The sandstones outcropped along the TFZ, were sampled around Çalören Village (Aksaray) (Figure 1, Line-A). The thickness of the sandstone sequence here is about 80 meters and consists of medium to thick-bedded, fine-medium-grained, and gray-yellowish-brown sandstones (Figure 4).

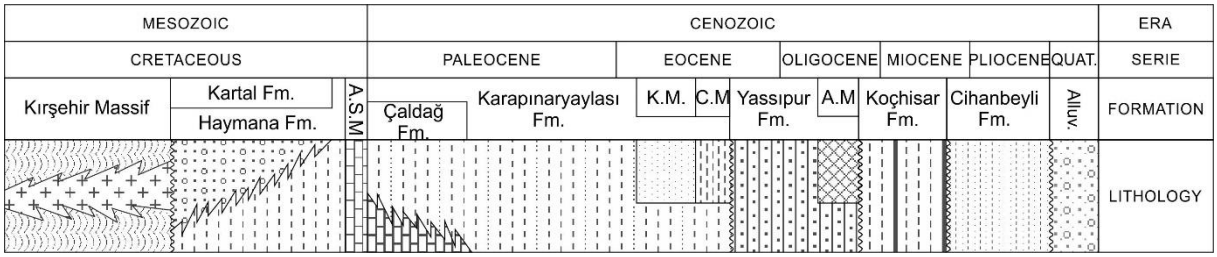

Figure 2. Generalized stratigraphic columnar section of the Tuzgölu Basin (adapted from [29]). Abbreviations; AM: Akbogaz Member, CM: Cavuşkalesi Member, KM: Karamollausagı Member, ASM: Asmayaylası Member.

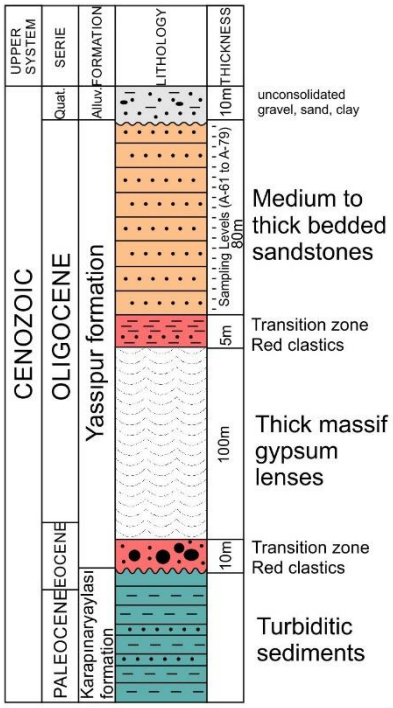

Figure 3. Generalized columnar section of the study area (unscaled).

2 Material and method

In the field, 19 samples were taken systematically (bottom to top) from the sandstone sequence. Petrographic thin sections were prepared following the standards and examined with a polarizing microscope. X-Ray Diffraction (XRD) analyses were performed in MTA Laboratories (Turkey). Samples were grounded by ceramic mortar and pestle. The powder samples were scanned with the Bruker D-8 Advance brand instrument using a 2.2 kW copper X-Ray anode between 10 and 70 degrees. Chemical concentrations of the elements were determined by Inductively Coupled Plasma-Emission Spectrometer (ICP-ES) for major elements and by Inductively Coupled Plasma-Mass Spectrometer (ICP-MS) for trace elements in ACME Labs (Canada). Solution samples were prepared by using the lithium borate fusion method. A 0.2 g weighed powder sample was poured into a graphite crucible and mixed with 1.5 g of $LiBO_2/Li_2B_4O_7$ flux. The mixture was melted in a muffle furnace for 30 minutes at 980 ˚C. Immediately after being poured into 100 mL of 5 % HNO_3 (ACS grade nitric acid diluted by distilled water) and mixed to dissolve completely. The solution samples were vaporized into an ICP emission spectrograph (ICP-ES; Spectro Ciros Vision) and ICP-MS (Perkin-Elmer Elan 6000 or 9000) for chemical analysis. The Loss on Ignition (LOI) was calculated by the weight difference for 1 g. sample after ignition at 950˚C for 90 minutes. Chondrite [30] and Post Archean Australian Shale (PAAS) [31] contents were used for normalization. Ce and Eu anomalies were calculated with the formulas $Ce/Ce^{*}= Ce_{cn} / [(La_{cn}).(Pr_{cn})]^{1/2}$ and $Eu/Eu^{*}= Eu_{cn} / [(Sm_{cn}).(Gd_{cn})]^{1/2}$ (cn: chondrite normalized).

Figure 4. Field photographs of the medium to thick-bedded and grey, yellow to brown coloured sandstones.

3 Results and discussion

3.1 Detrital petrography

In the thin sections, detrital components were composed of quartz %33-40 (avg. %37), feldspars (alkali felspar and plagioclase) %10-20 (avg. %15), rock fragments %15-30 (avg. %23), biotite %1-2 (avg. %1.5) and opaque minerals %3-7 (avg. %5) (Figure 5). Rock fragments include magmatic (andesite and dacite) and metamorphic (polycrystalline quartz) fragments. These framework grains were cemented by micrite (calcite). Foraminifera and red algae fossils can be observed within cement between the grains. According to Folk [32], sandstones were classified as feldspathic litharenite. XRD analyses show abundances of quartz, plagioclase, and calcite minerals (Figure 6).

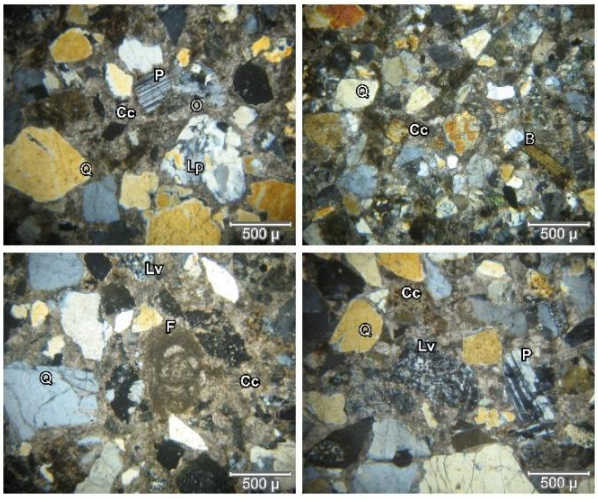

Figure 5. Micro photos of sandstone samples (cross nicols). Q: quartz, P: plagioclase, O: orthoclase, B: biotite, Lp: polycrystalline quartz, Lv: volcanic rock fragments, F: fossils and Cc: micrite.

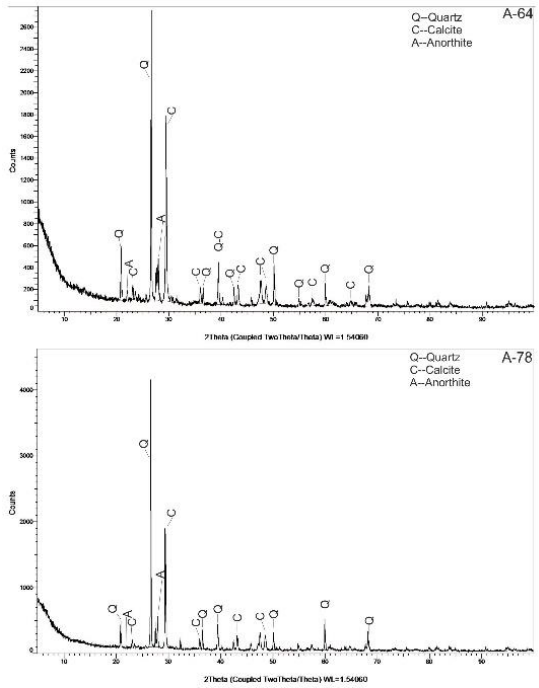

Figure 6. XRD analysis of A-64 and A-78 samples.

3.2 *Geochemistry*

Major and trace element concentrations of sandstone samples are arranged in Table 1. Compared to PAAS, SiO_2, Al_2O_3, Fe_2O_3, MgO, K_2O, TiO_2, P_2O_5, MnO and Cr_2O_3 concentrations were depleted, Na_2O remained unchanged and CaO was highly enriched (Figure 7a). Of the trace element concentrations, Mo is enriched while Sc, Ba, Co, Cs, Ga, Hf, Nb, Rb, Sr, Th, U, V, W, Zr, Y, Cu, Pb, Zn, and Ni are depleted (Figure 7b).

The chemical composition of clastic sediments is closely related to their grain size such that Al_2O_3 increases towards clay and SiO_2 towards the sand. In this order, other major oxides behave like Al_2O_3. This feature can give a strong prediction about the grain size and mineralogical composition of the clastic sediment [33]. Therefore, SiO_2/Al_2O_3 ratios are low in fine clastic sediments rich in clay minerals and high in coarse clastic sediments rich in quartz minerals. SiO_2/Al_2O_3 ratios of sandstone samples (avg. 8.07 ± 1.14) are higher than that of PAAS (3.32) but closer to average sandstone (10.93) of Pettijohn et al. [34].

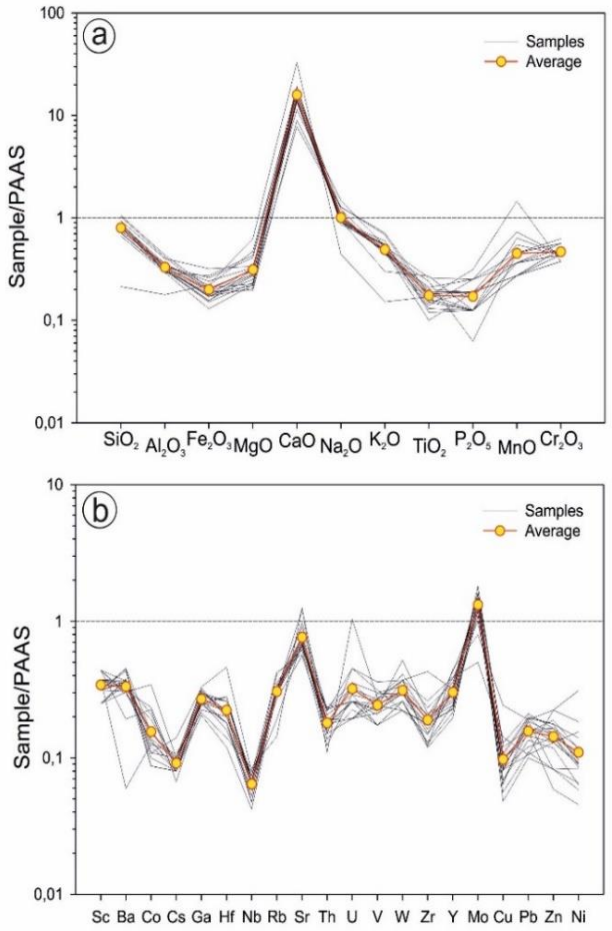

Figure 7. PAAS normalized diagrams **(a)** major elements and **(b)** trace elements.

3.3 *Rare earth elements*

The average, REE contents of the sandstone samples were 31.37 ± 5.71 ppm, Light REE (LREE) contents were 26.47 ± 5.39 ppm, and Heavy REE (HREE) contents were found to be 4.55 ± 0.89 ppm. These values show that REE concentrations were highly depleted compared to PAAS (Figure 8). The low abundance of REE indicates that the sandstones are immature [35]. According to the average $(La/Yb)_{cn}$, $(La/Sm)_{cn}$, and $(Gd/Lu)_{cn}$ ratios, REE was moderately fractionated according to the PAAS (Table 1). The average of Eu anomaly is 0.99 ± 0.10. This value shows that the Eu anomaly has a low negative effect. The average Ce anomaly is 0.94 ± 0.07. Also, this value shows that the Ce anomaly has a low negative effect. According to these features, the chondrite normalized average REE pattern has a slightly steep LREE, nearly flat HREE, and low negative Eu anomaly compared to PAAS.

Table 1. Major (%wt) and trace element (ppm) concentrations and some ratios.

El./Samp.	**A-61**	**A-62**	**A-63**	**A-64**	**A-65**	**A-66**	**A-67**	**A-68**	**A-69**	**A-70**	**A-71**
SiO_2	58.78	51.62	47.30	46.77	45.04	44.62	64.47	66.42	51.50	13.42	49.39
Al_2O_3	7.57	5.86	6.38	6.73	5.85	5.71	7.83	8.20	5.52	3.36	6.34
Fe_2O_3	2.31	1.13	1.26	1.58	1.12	1.32	1.39	1.50	0.94	1.61	1.88
MgO	0.74	0.60	0.72	1.04	0.69	0.48	0.43	0.50	0.49	1.38	0.90
CaO	14.74	21.01	22.45	22.15	24.49	24.60	11.62	10.09	21.16	42.62	20.82
Na_2O	1.77	1.22	1.25	1.45	1.20	1.09	1.54	1.53	1.10	0.53	1.31
K_2O	1.95	1.72	1.77	1.71	1.69	1.77	2.54	2.63	1.76	0.56	1.63
TiO_2	0.26	0.18	0.16	0.24	0.13	0.14	0.16	0.18	0.10	0.17	0.21
P_2O_5	0.04	0.03	0.02	0.01	0.02	0.04	0.02	0.03	0.03	0.05	0.04
MnO	0.05	0.04	0.03	0.05	0.03	0.04	0.05	0.03	0.03	0.16	0.08
Cr_2O_3	0.009	0.008	0.007	0.009	0.008	0.007	0.010	0.006	0.006	0.006	0.007
LOI	11.7	16.5	18.6	18.2	19.6	20.1	9.8	8.8	17.3	36.0	17.3
Sum	99.87	99.89	99.92	99.90	99.90	99.92	99.90	99.90	99.95	99.90	99.90
TOT/C	2.70	4.10	4.59	4.69	5.24	4.92	2.39	2.08	4.44	8.90	4.44
SiO_2/Al_2O_3	7.76	8.81	7.41	6.95	7.70	7.81	8.23	8.10	9.33	3.99	7.79
Sc	6	4	6	7	4	5	5	5	4	6	7
Ba	227	225	213	188	197	231	293	288	239	39	197
Co	4.8	2.8	3.5	4.4	3.0	3.5	3.5	2.5	2.0	2.9	7.9
Cs	1.3	1.2	1.4	1.4	1.3	1.5	1.5	2.1	1.2	1.6	1.5
Ga	6.6	4.5	5.1	5.6	5.1	4.9	6.3	6.5	4.1	4.3	6.2
Hf	2.3	1.0	1.4	1.3	0.8	0.9	1.0	1.0	0.6	0.7	1.1
Nb	1.5	1.2	1.2	1.3	1.1	1.0	1.2	1.4	0.8	1.6	1.4
Rb	52.4	48.5	50.7	47.3	48.0	50.2	65.3	67.4	48.0	22.9	45.9
Sr	181.1	244.3	130.7	194.9	146.3	151.7	124.6	114.0	124.9	250.6	157.2
Th	3.0	2.6	3.4	3.3	2.0	2.3	3.4	3.3	1.8	1.6	3.2
U	0.9	0.8	1.1	1.0	0.7	0.8	0.8	0.8	0.9	3.2	1.4
V	39	26	35	40	26	26	31	37	26	41	47
W	1.0	0.6	1.4	1.1	0.7	0.7	1.0	0.8	0.7	1.0	0.6
Zr	89.8	36.6	44.3	48.8	27.3	38.2	41.8	40.4	25.0	25.4	37.4
Mo	1.6	1.8	1.5	1.4	1.3	1.2	1.8	1.1	1.5	0.8	1.2
Cu	6.4	6.0	4.6	5.0	4.3	4.1	5.2	3.2	3.4	12.1	4.9
Pb	4.2	3.2	3.4	3.1	3.2	3.7	3.9	3.7	3.1	3.8	2.9
Zn	14	14	11	16	13	7	15	13	5	19	11
Ni	6.5	5.3	4.9	6.4	5.3	4.6	4.9	5.7	2.5	17.1	8.5
As	2.9	2.9	2.6	1.2	1.8	1.8	1.8	3.0	2.8	1.4	2.9
Sb	0.4	0.3	0.4	0.4	0.2	0.2	0.2	0.2	0.2	0.2	0.3
Y	8.6	6.2	7.7	9.6	6.6	6.1	6.9	6.5	5.3	12.0	11.6
La	7.4	9.4	8.9	8.8	5.6	5.3	7.6	7.7	4.5	5.5	7.8
Ce	14.0	16.5	16.0	16.1	10.5	9.5	14.2	15.0	8.5	10.0	14.1
Pr	1.58	1.72	1.84	1.75	1.12	1.07	1.58	1.61	0.96	1.18	1.60
Nd	6.2	5.4	6.6	6.4	3.9	4.1	6.1	5.6	3.8	4.8	6.3
Sm	1.19	0.99	1.19	1.17	0.87	0.89	1.16	0.96	0.74	1.13	1.20
Eu	0.41	0.33	0.37	0.38	0.31	0.29	0.39	0.39	0.29	0.33	0.37
Gd	1.21	1.02	1.21	1.21	0.89	0.84	1.17	1.02	0.74	1.39	1.42
Tb	0.23	0.16	0.19	0.23	0.15	0.15	0.18	0.17	0.14	0.25	0.24
Dy	1.31	0.89	1.11	1.38	0.94	0.84	1.11	1.00	0.78	1.42	1.48
Ho	0.29	0.20	0.24	0.32	0.21	0.20	0.22	0.22	0.17	0.33	0.34
Er	0.85	0.68	0.77	0.97	0.66	0.57	0.69	0.71	0.52	1.07	1.09
Tm	0.14	0.10	0.12	0.16	0.11	0.10	0.11	0.11	0.09	0.17	0.17
Yb	0.94	0.59	0.75	0.93	0.58	0.63	0.73	0.70	0.50	0.99	1.03
Lu	0.16	0.10	0.12	0.15	0.10	0.09	0.12	0.10	0.08	0.17	0.17
ΣREE	35.91	38.08	39.41	39.95	25.94	24.57	35.36	35.29	21.81	28.73	37.31
$(La/Yb)_{cn}$	5.45	11.03	8.22	6.55	6.68	5.82	7.21	7.62	6.23	3.85	5.24
$(La/Sm)_{cn}$	3.90	5.95	4.69	4.71	4.03	3.73	4.11	5.03	3.81	3.05	4.07
$(Gd/Lu)_{cn}$	0.93	1.26	1.25	1.00	1.10	1.15	1.21	1.26	1.14	1.01	1.03
$(Ce/Ce^*)_{cn}$	0.98	0.98	0.95	0.98	1.01	0.96	0.98	1.02	0.98	0.94	0.96
$(Eu/Eu^*)_{cn}$	1.04	1.00	0.94	0.97	1.07	1.02	1.02	1.20	1.19	0.80	0.86

Table 1. Major (%wt) and trace element (ppm) concentrations and some ratios (continued).

El./Samp.	A-72	A-73	A-74	A-75	A-76	A-77	A-78	A-79	Average	PAAS
SiO_2	50.65	55.51	54.48	55.72	52.96	41.75	53.02	51.19	50.24	62.80
Al_2O_3	5.78	6.13	6.74	6.38	6.11	5.52	6.34	5.96	6.23	18.90
Fe_2O_3	1.09	1.24	1.49	1.37	1.23	1.97	1.74	1.23	1.44	7.23
MgO	0.51	0.45	0.67	0.62	0.55	0.95	0.72	0.61	0.69	2.20
CaO	20.97	17.73	17.91	17.54	19.15	24.93	18.36	20.15	20.66	1.30
Na_2O	1.04	1.09	1.12	1.17	1.09	1.13	1.19	1.16	1.21	1.20
K_2O	2.00	2.21	2.05	1.94	2.02	1.11	1.73	1.73	1.82	3.70
TiO_2	0.13	0.12	0.19	0.18	0.15	0.27	0.20	0.15	0.17	1.00
P_2O_5	0.02	0.02	0.03	0.02	0.03	0.02	0.03	0.02	0.03	0.16
MnO	0.03	0.04	0.04	0.04	0.03	0.07	0.06	0.04	0.05	0.11
Cr_2O_3	0.007	0.007	0.007	0.007	0.008	0.007	0.007	0.009	0.007	0.016
LOI	17.7	15.4	15.2	14.9	16.6	22.2	16.5	17.7	17.37	6.00
Sum	99.91	99.91	99.90	99.91	99.91	99.91	99.92	99.92	99.91	104.59
TOT/C	4.44	3.67	3.75	3.76	4.01	5.49	3.89	4.32	4.44	3.67
SiO_2/Al_2O_3	8.76	9.06	8.08	8.73	8.67	7.56	8.36	8.59	8.07	3.32
Sc	4	5	7	6	5	7	6	5	5.47	16.00
Ba	245	280	238	236	237	125	200	199	215.63	650.00
Co	2.3	2.0	3.2	3.5	2.5	5.2	5.4	3.1	3.58	23.00
Cs	1.2	1.2	1.4	1.4	1.5	1.0	1.2	1.2	1.37	15.00
Ga	5.3	5.1	6.0	6.0	5.1	4.9	5.8	5.1	5.39	-
Hf	0.9	1.1	1.1	1.3	0.9	1.4	1.3	1.1	1.12	5.00
Nb	0.9	0.9	1.3	1.3	1.1	1.3	1.4	1.3	1.22	19.00
Rb	51.7	56.5	52.0	50.4	52.4	30.5	43.1	46.7	48.94	160.00
Sr	156.1	133.5	135.9	131.2	140.5	140.8	111.1	131.6	152.68	200.00
Th	2.2	2.5	2.8	2.8	2.6	2.2	2.4	2.6	2.63	14.60
U	0.6	0.8	0.6	0.6	0.6	1.4	1.1	0.8	0.99	3.10
V	32	34	44	41	36	54	45	33	36.47	150.00
W	0.7	0.8	0.8	0.8	0.6	1.0	0.9	0.8	0.84	-
Zr	26.6	31.8	33.9	43.5	31.2	54.9	42.8	35.9	39.77	210.00
Mo	1.4	1.6	1.3	1.2	1.3	0.5	1.0	1.6	1.32	-
Cu	2.8	2.4	4.2	4.0	3.4	7.1	5.4	4.1	4.87	50.00
Pb	2.2	2.0	2.4	3.9	2.7	2.1	4.0	2.1	3.14	20.00
Zn	7	7	12	12	10	19	15	11	12.16	85.00
Ni	3.6	3.2	5.0	4.7	3.5	10.1	7.7	5.1	6.03	55.00
As	1.6	2.1	2.4	2.5	2.6	1.6	4.1	1.9	2.31	-
Sb	0.2	0.2	0.2	0.2	0.2	0.2	0.4	0.2	0.25	-
Y	5.8	8.3	8.7	7.2	8.2	10.5	10.3	9.1	8.17	27.00
La	5.4	7.4	7.6	6.1	6.6	5.0	6.1	5.4	6.74	38.00
Ce	9.0	12.0	12.3	11.5	10.8	7.8	12.4	9.3	12.08	80.00
Pr	1.07	1.58	1.55	1.29	1.40	1.13	1.40	1.16	1.40	8.83
Nd	3.8	5.7	6.0	4.9	5.5	4.3	5.7	3.9	5.21	32.00
Sm	0.80	1.13	1.25	0.99	1.06	0.97	1.16	0.95	1.04	5.60
Eu	0.28	0.36	0.38	0.31	0.36	0.34	0.37	0.33	0.35	1.10
Gd	0.81	1.18	1.36	0.99	1.15	1.21	1.34	1.17	1.12	4.70
Tb	0.14	0.20	0.23	0.18	0.19	0.23	0.23	0.21	0.19	0.77
Dy	0.84	1.09	1.19	1.06	1.20	1.45	1.38	1.26	1.14	4.40
Ho	0.17	0.25	0.27	0.22	0.26	0.34	0.32	0.27	0.25	1.00
Er	0.55	0.72	0.78	0.73	0.76	1.04	1.00	0.89	0.79	2.90
Tm	0.09	0.12	0.13	0.11	0.12	0.17	0.15	0.14	0.13	0.405
Yb	0.56	0.69	0.78	0.75	0.79	1.01	1.02	0.92	0.78	2.80
Lu	0.09	0.12	0.13	0.12	0.13	0.18	0.16	0.15	0.13	0.40
ΣREE	23.60	32.54	33.95	29.25	30.32	25.17	32.73	26.05	31.37	182.91
$(La/Yb)_{cn}$	6.68	7.43	6.75	5.63	5.78	3.43	4.14	4.06	6.20	9.40
$(La/Sm)_{cn}$	4.23	4.10	3.81	3.86	3.90	3.23	3.30	3.56	4.06	4.25
$(Gd/Lu)_{cn}$	1.11	1.22	1.29	1.02	1.09	0.83	1.04	0.96	1.10	1.45
$(Ce/Ce^*)_{cn}$	0.90	0.84	0.86	0.98	0.85	0.79	1.02	0.89	0.94	1.05
$(Eu/Eu^*)_{cn}$	1.06	0.95	0.89	0.95	0.99	0.95	0.90	0.95	0.99	0.65

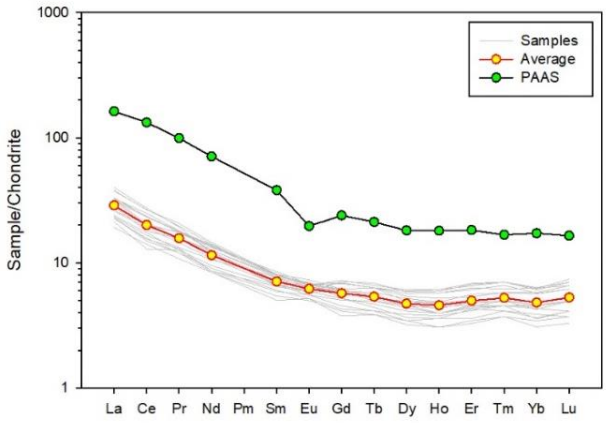

Figure 8. Comparison of REE contents with PAAS.

The Ce anomaly is useful in determining the redox conditions of the environment [36]. Ce is found in terrestrial sedimentary rocks and igneous rocks in trivalent state like other REEs [37]. However, at the oxygen-rich upper level of seawater, Ce+3 oxidizes to Ce+4, which is highly insoluble in water, causing it to separate from the other REEs. In anoxic or suboxic environments, on the contrary, it is reduced from insoluble Ce+4 to Ce+3 [38].

Ce anomaly took values between 0.95 and 1.05 in the lower part (A-61 to A-71) of the sequence (Figure 9). In this part, the amounts of variations between the samples are small. However, the Ce anomaly takes values between 0.80 and 1.00 in the upper part of the sequence (A-72 to A-79). In this part, the amounts of variations between samples are greater when compared with the lower part. The instability that has occurred between the lower and upper parts of the sequence indicates that there has been variation in the oxygen level of the water during deposition.

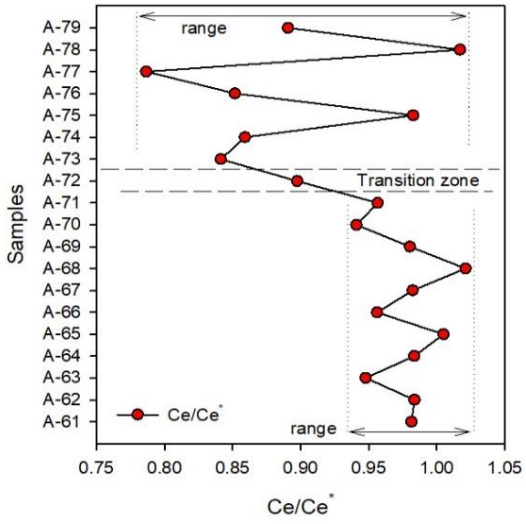

Figure 9. Ce anomaly variations along the sequence.

3.4 Correlation coefficients

Correlation coefficients are useful in determining the belongings of the elements. The matrix of the significant positive and negative correlation coefficients is arranged in Table 2. Strong positive correlations of Na_2O and K_2O with Al_2O_3 and SiO_2, respectively, indicate that they are associated with feldspars. The strong positive correlation between Al_2O_3 and SiO_2 indicates that the grain size contrast is insignificant, that is, the grains are well sorted. There is a very strong positive correlation between Total Carbon (TOTC) and CaO. Accordingly, the carbon concentration is mostly related to calcite (cement) in the diagenetic phase. MgO and MnO, which have strong positive correlations with CaO, are also associated with cement. The strong positive correlation between CaO and Loss on Ignition (LOI) indicates that LOI is mostly of calcite origin. Strong negative correlation between CaO and SiO_2 indicates that CaO and SiO_2 are inversely proportional. The variations in SiO_2 concentrations in the samples are controlled by diagenetic calcite. Strong positive correlation of Sc with Fe_2O_3, MgO, and TiO_2 may indicate its association with ferromagnesian or heavy minerals. The strong positive correlation of Ba with SiO_2, Al_2O_3, and K_2O may indicate its association with K-feldspars. The strong positive correlation of Co with Fe_2O_3 and TiO_2 may associate it with heavy minerals. The strong positive correlation between U and CaO shows the relation of U with cement. The strong positive correlation of Zr with Fe_2O_3 and TiO_2 indicates its association with heavy minerals. The strong positive correlation between Fe_2O_3 and TiO_2 may show their association with biotite. The strong positive correlations of Cu and Ni with MgO, CaO, and LOI may indicate that they are associated with diagenesis and behave according to the redox conditions of the environment [39]. The strong positive correlation of Rb with SiO_2 and Al_2O_3 indicates that it is associated with clastics. The strong positive correlation of Sr with LOI indicates that it is related to the diagenetic phase. The strong positive correlation of Hf with Zr indicates its relationship with zircon mineral.

3.5 Provenance

The SiO_2 concentrations of the samples are controlled by the random concentrations of diagenetic CaO. This affects the major oxide composition of the clastic phase, making provenance and tectonic setting diagrams using major oxide concentrations useless for the sandstones. Therefore, it is more appropriate to use trace element diagrams for the sandstones in this study.

The Zr/Sc vs. Th/Sc diagram is frequently used to evaluate the effect of sedimentary recycling [40]. The Th/Sc ratio is a general indicator of provenance and Zr/Sc is an index used to determine zircon enrichment. The first cycle sediments show a positive correlation with the compositional variation line in the diagram. But an increase in the Zr/Sc ratio is observed in the recycled sediments. Sandstone samples don't cross to the right of the compositional variations line in the diagram and cluster closely to the andesite composition. The lack of shift in the direction of the Zr/Sc axis indicates that the sandstones didn't experience sedimentary recycling (Figure 10). In this sense, sandstones are first cycle sediments transported directly from the source.

Table 2. Matrix of correlation coefficients.

N=19	SiO_2	Al_2O_3	Fe_2O_3	MgO	CaO	Na_2O	K_2O	TiO_2	MnO	LOI	TOTC	Sc	Ba	Co	Hf	Sr	Th	U	Zr	Cu	Ni
SiO_2																					
Al_2O_3	.90																				
Fe_2O_3	-.05	.22																			
MgO	-.78	-.52	.51																		
CaO	-1.00	-.93	-.03	.73																	
Na_2O	.77	.91	.37	-.34	-.79																
K_2O	.93	.85	-.23	-.82	-.92	.64															
TiO_2	-.02	.25	.88	.54	-.06	.42	-.24														
MnO	-.77	-.59	.45	.83	.73	-.50	-.75	.30													
LOI	-.99	-.93	.00	.74	.99	-.82	-.92	-.04	.75												
TOTC	-.99	-.93	-.04	.74	.99	-.81	-.92	-.05	.72	1.00											
Sc	-.18	.08	.73	.61	.11	.10	-.29	.76	.42	.15	.13										
Ba	.92	.76	-.33	-.91	-.89	.58	.97	-.34	-.81	-.90	-.90	-.39									
Co	-.04	.14	.74	.43	-.01	.31	-.26	.69	.32	.00	.01	.69	-.29								
Hf	.29	.46	.74	.12	-.34	.63	.09	.73	-.07	-.34	-.37	.49	.04	.46							
Sr	-.61	-.49	.13	.60	.62	-.28	-.58	.23	.57	.56	.56	.02	-.56	.01	-.02						
Th	.62	.81	.27	-.18	-.65	.76	.60	.37	-.32	-.66	-.66	.37	.49	.33	.48	-.23					
U	-.83	-.65	.34	.83	.80	-.54	-.79	.20	.96	.81	.79	.33	-.84	.21	-.13	.56	-.36				
Zr	.28	.49	.78	.13	-.33	.69	.08	.76	-.03	-.34	-.37	.43	.03	.46	.95	.04	.45	-.09			
Cu	-.75	-.53	.47	.83	.71	-.35	-.77	.43	.90	.71	.68	.35	-.84	.26	.09	.68	-.29	.89	.17		
Ni	-.76	-.52	.54	.89	.70	-.40	-.77	.46	.95	.73	.71	.48	-.87	.38	.03	.55	-.27	.93	.08	.93	

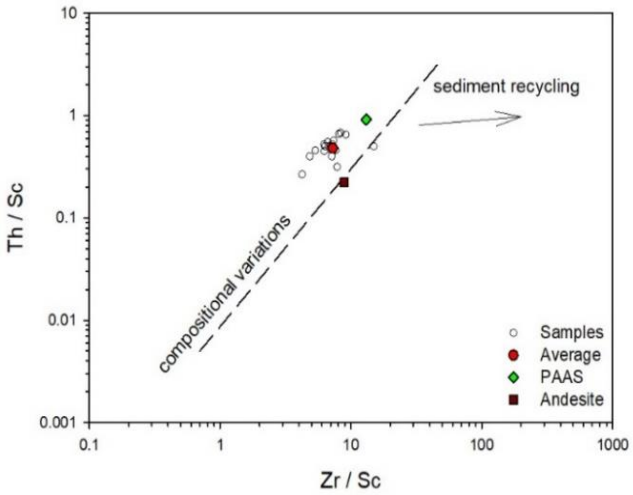

Figure 10. Th/Sc-Zr/Sc diagram [40].

In addition to traditional petrographic methods [41-43], geochemical methods are also used as the major method for provenance extraction [44-49]. Y, La, Th, Zr, Sc, Co, Ni, Cr, Hf, V, and REE are useful determinants for provenance analysis as they are transferred from source to sediment mostly unchanged during sedimentary processes [50-53]. REE patterns and Eu anomaly sizes of post-Archean clastic deposits are of particular importance as an indicator of provenance [40]. The main reason for this is that basic rocks have lower LREE/HREE ratios and no negative Eu anomalies, while more silicic rocks have higher LREE/HREE ratios and significant negative Eu anomalies [54]. Eu depletion in post-Archean sedimentary rocks is not an event resulting from surface processes, but evidence of an earlier magmatic event resulting from the retention of Eu in Ca-rich plagioclase in the lower crust. Therefore, igneous rocks derived from the mantle rarely show negative Eu anomalies [55]. For the sandstones, slightly inclined REE patterns and low negative Eu anomalies indicate the existence of plagioclase-rich magmatic rocks in the source region that is not significantly affected by intra-crustal fractionation.

Th and Sc are effective elements for provenance diagnosis [31]. In the Th/Sc vs. Eu/Eu^* binary diagram, a line representing average igneous rock compositions can be obtained [56]. This line is very useful for estimating provenance. In the diagram, sandstone samples cluster close to the average andesite composition (Figure 11).

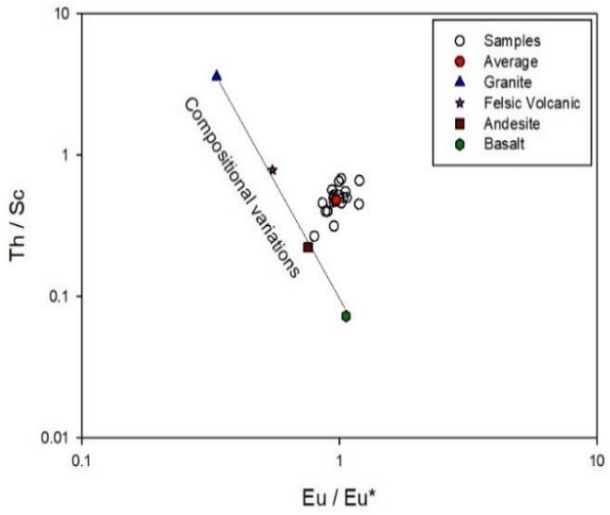

Figure 11. Eu/Eu^*-Th/Sc binary diagram [56]. Compositional variations were taken from [57].

Comparison of some trace element ratios sensitive to provenance with average igneous rock compositions is very useful for revealing the composition of source [58-62]. In this sense, the average ratios of sandstone samples such as La/Sc, La/Co, Th/Sc, Th/Co, Th/Cr, Zr/Sc, Zr/Co, Ba/Sc, and Ba/Co and average igneous rock compositions of Condie [57] were compared (Table 3). This comparison reveals that the sandstones are close to the average andesite composition.

The magmatic and metamorphic complex of the Kırşehir Massif around the study area is the most likely source of sandstones [63-67]. Görür et al. [12], stated that the western end of the Tuzgölü basin faced the closing Inner Taurus Ocean so that the material transportation to the basin was from the Kırşehir Block at the east.

Table 3. Critical element ratios for provenance.

Rat/Roc.	*Granite	*Felsic Volcanic	*Andesite	*Basalt	This study
La/Sc	8.00	2.15	1.11	0.33	1.23
La/Co	13.33	4.67	0.91	0.31	1.88
Th/Sc	3.60	0.78	0.22	0.07	0.48
Th/Co	6.00	1.70	0.18	0.07	0.74
Th/Cr	2.25	2.04	0.08	0.02	0.05
Zr/Sc	50.00	16.54	8.89	3.97	7.27
Zr/Co	83.33	35.83	7.27	3.74	11.11
Ba/Sc	160.00	65.38	36.11	12.42	39.39
Ba/Co	266.67	141.67	29.55	11.71	60.25

* Data from [57]

3.6 Tectonic setting

The mineralogical and geochemical compositions of the sediments deposited in a basin are closely related to the composition and tectonic setting of the source rocks [68, 69]. Accordingly, many discrimination diagrams have been derived which determine the tectonic setting by using the major and trace element contents of the deposited sediments [70-73].

Trace element diagrams of Bhatia, and Crook [72] were found reliable by LaMaskin et al. [74] (Figure 12). In these triangular diagrams (La-Th-Sc, Th-Co-Zr/10, and Th-Sc-Zr/10) tectonic settings are divided into four. These are A-Oceanic Island Arc (forearc, back-arc), B-Continental Island Arc (apical inter-arc, forearc, back-arc), C-Active Continental Margin (retro-arc foreland, marginal basins, oblique-slip basins), and D-Passive Continental Margin (major peri-cratonic depocentres on trailing edges). In all three diagrams, the sample average falls on the "Continental Island Arc" region.

While constructing the tectonic model of the Tuzgölü basin, Görür et al. [12], suggested the existence of the Inner Tauride Ocean between the Menderes Taurus Block and the Kırşehir Block (Figure 13). According to this tectonic model, the Tuzgölü basin developed as a forearc basin with the subduction of the Inner Taurus Ocean under the Kırşehir Block. The Continental Island Arc tectonic setting obtained from the diagrams represents a subduction event at the continental margin. Therefore, the tectonic setting of the samples supports the presence of the Inner Taurus Ocean and the fore-arc basin model proposed by Görür et al. [12].

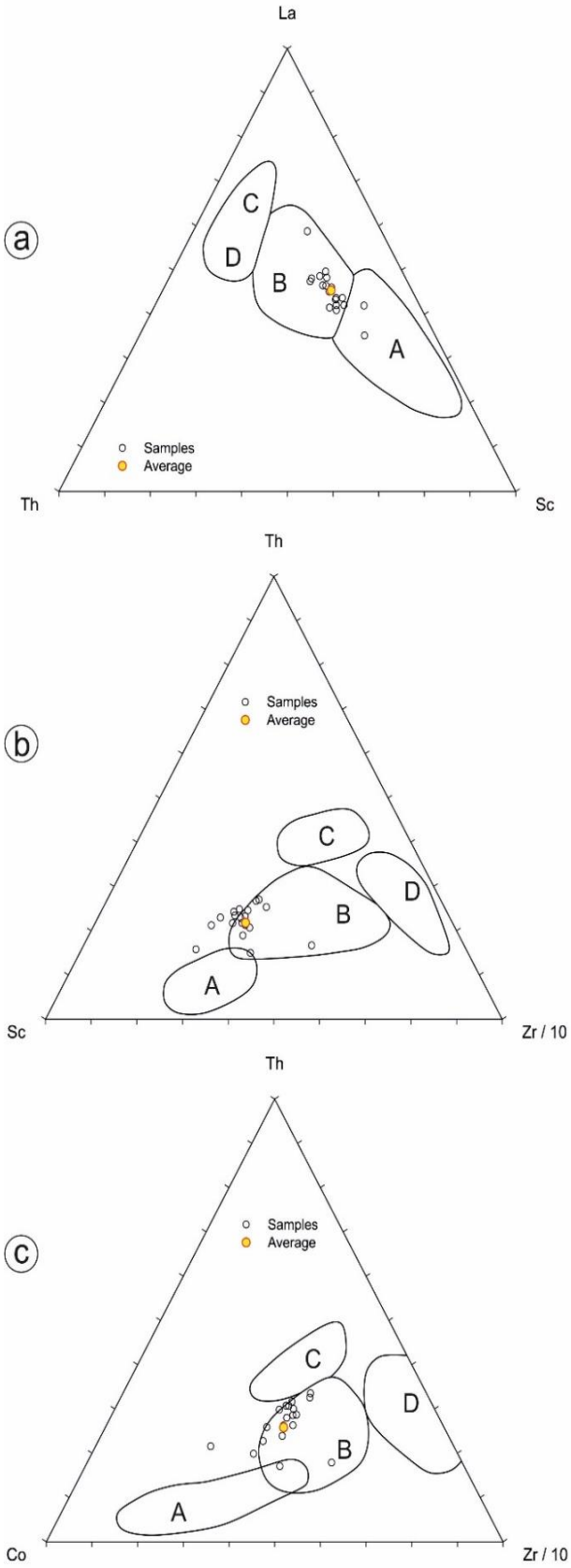

Figure 12. Ternary plots of **(a)** La-Th-Sc, **(b)** Th-Sc-Zr/10 and **(c)** Th-Co-Zr/10 [72]. A-Oceanic Island Arc, B-Continental Island Arc, C-Active Continental Margin, and D-Passive Margin.

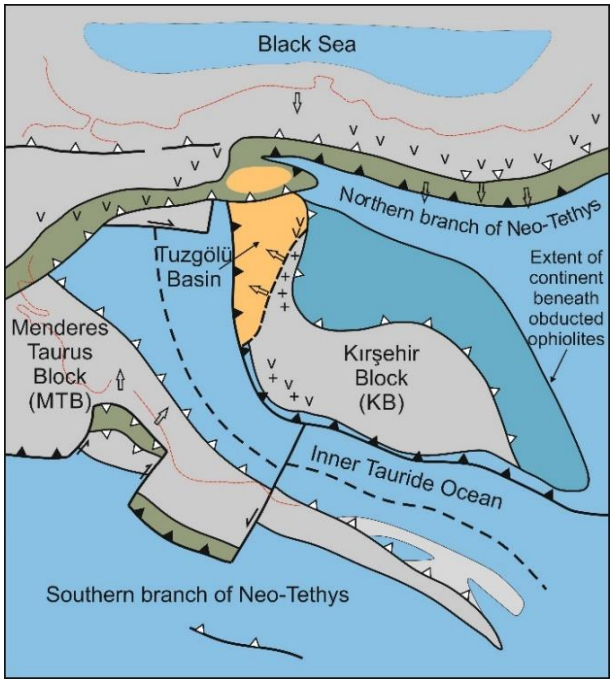

Figure 13. Paleocene paleogeography around Tuzgölü Basin after Görür et al. [12]. Note the existence of the Inner Tauride Ocean.

4 Conclusions

Sandstones are classified as feldspathic litharenite. Quartz, plagioclase, and calcite minerals were detected in the XRD analysis. According to the Zr/Sc-Th/Sc diagram, no sedimentary recycling is observed. This shows that these sandstones are first cycle sediments transported directly from the source. The fact that the sandstones are the first cycle, increases the reliability of the diagrams used. REE contents were considerably depleted when compared to PAAS. The variation in the negative Ce anomaly effect along the sequence indicates that oxygen level in the water variated during deposition. Critical element ratios for provenance such as La/Sc, La/Co, Th/Sc, Th/Co, Th/Cr, Zr/Sc, Zr/Co, Ba/Sc, and Ba/Co, Th/Sc-Eu/Eu* diagram and average REE pattern suggest provenance in "intermediate magmatic" composition for the sandstones. La-Th-Sc, Th-Co-Zr/10 and Th-Sc-Zr/10 diagrams give the "Continental Island Arc" tectonic setting for the samples. This setting describes an arc that developed on the continental margin of the subduction zone. Provenance analyses also support the existence of this arc by pointing to a source with an intermediate composition rather than a cratonic source. The tectonic setting proposed for the sandstones in this study supports the tectonic model that the Tuzgölü basin was a fore-arc basin adjacent to the Kırşehir Block.

Acknowledgments

This study is derived from some part of the first author's Ph.D thesis, which was financially supported by Selçuk University Research Fund (09101002, BAP). Authors would like to thank the reviewers for their constructive criticism and valuable contributions to the study.

Conflict of interest

The authors of the study declare that there is no conflict of interest.

Similarity rate (iThenticate): %12

References

[1] A. Aydemir, Hydrocarbon potential of the Tuzgolu (Salt Lake) Basin, Central Anatolia, Turkey: A comparison of geophysical investigation results with the geochemical data. Journal of Petroleum Science and Engineering, 61 (1), 33-47, 2008. http://dx.doi.org/10.1016/j.petrol.2007.10.004

[2] A. Aydemir, Tectonic investigation of Central Anatolia, Turkey, using geophysical data. Journal of Applied Geophysics, 68, 321-334, 2009.

[3] A. Aydemir and A. Ateş, Interpretation of Suluklu-Cihanbeyli-Goloren magnetic anomaly, Central Anatolia, Turkey: An integration of geophysical data. Physics of the Earth and Planetary Interiors, 159 (3–4), 167-182, 2006. http://dx.doi.org/10.1016/j.pepi.2006.06.007

[4] C. Gürbüz and J. R. Evans, A seismic refraction study of the western Tuz Gölü basin, central Turkey. Geophysical Journal International, 106 (1), 239-251, 1991. https://doi.org/10.1111/j.1365-246X.1991.tb04614.x.

[5] H. Ü. Ercan, M. Ç. Karakaya, A. Bozdağ, N. Karakaya and A. Delikan, Origin and evolution of halite based on stable isotopes (δ37Cl, δ81Br, δ11B and δ7Li) and trace elements in Tuz Gölü Basin, Turkey. Applied Geochemistry, 105, 17-30, 2019. https://doi.org/10.1016/j.apgeochem.2019.04.008.

[6] K. Dirik and M. C. Göncüoglu, Neotectonic characteristics of Central Anatolia. International Geology Review, 38 (9), 807-817, 1996. https://doi.org/10.1080/00206819709465363.

[7] E. Özsayin and K. Dirik, Quaternary activity of the Cihanbeyli and Yeniceoba fault zones: İnönü-Eskişehir fault system, Central Anatolia. Turkish Journal of Earth Sciences, 16 (4), 471-492, 2007.

[8] M. Y. Hüseyinca, Mineralogical and geochemical characteristics of the sediments in Lake Tuz and the close vicinity (in Turkish). Ph.D. Thesis, Selçuk University, Konya, 2015.

[9] A. Uygun and E. Şen, Tuz Gölü Havzası ve doğal kaynakları I: Tuz Gölü suyunun jeokimyası. Bulletin of the Geological Society of Turkey, 21, 113-120, 1978.

[10] K. Dirik and O. Erol, Tuzgölü ve civarının tektonomorfolojik evrimi Orta Anadolu, Türkiye. Türkiye Petrol Jeologları Derneği Özel Sayı, 5, 27-46, 2000.

[11] M. Clark and A. Robertson, The role of the Early Tertiary Ulukisla Basin, southern Turkey, in suturing of the Mesozoic Tethys Ocean. Journal of the Geological Society, 159 (6), 673-690, 2002.

[12] N. Görür, F. Y. Oktay, İ. Seymen and A. M. C. Şengör, Palaeotectonic evolution of the Tuzgölü basin complex, Central Turkey: sedimentary record of a Neo-Tethyan closure. In J. E. Dixon, A. H. F. Robertson (Eds.), The

geological evolution of the eastern mediterranean, pp. 467-482, Geological Society Special Publications, London, 1984.
[13] A. Koçyiğit, An example of an accretionary forearc basin from northern Central Anatolia and its implications for the history of subduction of Neo-Tethys in Turkey. Geological Society of America Bulletin, 103 (1), 22-36, 1991. https://doi.org/10.1130/00167606(1991)103<0022:aeoaaf>2.3.co;2.
[14] Y. Arıkan, Tuz Gölü havzasının jeolojisi ve petrol imkanları. M.T.A. Dergisi, 85, 17-38, 1975.
[15] I. Çemen, M. C. Göncüoglu and K. Dirik, Structural evolution of the Tuzgölü basin in Central Anatolia, Turkey. The Journal of geology, 107 (6), 693-706, 1999.
[16] M. Clark and A. Robertson, Uppermost Cretaceous–Lower Tertiary Ulukışla Basin, south-central Turkey: sedimentary evolution of part of a unified basin complex within an evolving Neotethyan suture zone. Sedimentary Geology, 173 (1), 15-51, 2005. https://doi.org/10.1016/j.sedgeo.2003.12.010.
[17] A. I. Okay and O. Tüysüz, Tethyan sutures of northern Turkey. Geological Society, London, Special Publications, 156 (1), 475-515, 1999.
[18] A. M. C. Şengör, Tectonics of the tethysides: orogenic collage development in a collisional setting. annual review of earth and planetary sciences, 15 (1), 213-244, 1987.
[19] G. M. Stampfli, The intra-alpine terrain: A paleotethyan remnant in the alpine variscides. Eclogae Geologicae Helvetiae, 89 (1), 13-42, 1996.
[20] A. M. C. Şengör and Y. Yilmaz, Tethyan evolution of Turkey: a plate tectonic approach. Tectonophysics, 75 (3), 181-241, 1981.
[21] A. Okay, Geology of Turkey: A Synopsis. Anschitt, 21, 19-42, 2008.
[22] N. Görür, O. Tüysüz and A. M. C. Şengör, Tectonic evolution of the Central Anatolian basins. International Geology Review, 40 (9), 831-850, 1998. https://doi.org/10.1080/00206819809465241.
[23] M. Şenel, Turkiye Jeoloji Haritası/Geological Map of Turkey, scale 1:500,000. Maden Tetkik Arama Genel Müdürlüğü, Ankara, 2002.
[24] İ. Seymen, Kaman dolayında Kırşehir Masifinin jeolojisi. Doçentlik Tezi, İ.T.Ü. Maden Fakültesi, İstanbul, 1982.
[25] A. Özcan, M. C. Göncüoğlu, N. Turan, Ş. Uysal, K. Şentük and A. Işık, Late Paleozoik evolution of the Kütahya-Bolkardağ Belt. METU Journal of Pure and Applied Sciences, 21 (1-3), 211-220, 1988.
[26] A. Uygun, Tuzgölü havzasının jeolojisi, evaporit oluşumları ve hidrokarbon olanakları. İç Anadolu'nun Jeolojisi Sempozyumu, T.J.K. 35. Bilimsel ve Teknik Kurultayı Bildiriler Kitabı, pp. 66-71, Ankara, 1981.
[27] E. Özsayin, T. A. Çiner, F. B. Rojay, R. K. Dirik, D. Melnick, D. Fernández-Blanco, G. Bertotti, T. F. Schildgen, Y. Garcin, M. R. Strecker and M. Sudo, Plio-Quaternary extensional tectonics of the Central Anatolian Plateau: A case study from the Tuz Gölü Basin, Turkey. Turkish Journal of Earth Sciences, 22 (5), 691-714, 2013.
[28] A. Kürçer and Y. E. Gökten, Paleoseismological three dimensional virtual photography method; A case study: Bağlarkayası-2010 trench, Tuz Gölü Fault Zone, Central Anatolia, Turkey. In E. Sharkov (Ed.), Tectonics - Recent Advances, IntechOpen, 2012.
[29] A. Aydemir and A. Ateş, Structural interpretation of the Tuzgolu and Haymana Basins, Central Anatolia, Turkey, using seismic, gravity and aeromagnetic data. Earth Planets and Space, 58 (8), 951-961, 2006.
[30] E. Anders and N. Grevesse, Abundances of the elements: Meteoritic and solar. Geochimica et Cosmochimica Acta, 53 (1), 197-214, 1989. http://dx.doi.org/10.1016/0016-7037(89)90286-X.
[31] S. R. Taylor and S. M. McLennan, The continental crust: Its composition and evolution. Blackwell Scientific Publications, Oxford, 1985.
[32] R. L. Folk, Petrology of sedimentary rocks. Hemphill Publishing Company, Austin, Texas, 1974.
[33] H. Vital and K. Stattegger, Major and trace elements of stream sediments from the lowermost Amazon River. Chemical geology, 168 (1–2), 151-168, 2000. http://dx.doi.org/10.1016/S0009-2541(00)00191-1.
[34] F. J. Pettijohn, P. E. Potter and R. Siever, Sand and sandstone. Springer US, New York, 1972.
[35] R. L. Cullers, T. Barrett, R. Carlson and B. Robinson, Rare-earth element and mineralogic changes in Holocene soil and stream sediment: A case study in the Wet Mountains, Colorado, U.S.A. Chemical geology, 63 (3–4), 275-297, 1987. http://dx.doi.org/10.1016/0009-2541(87)90167-7.
[36] H. Elderfield and M. J. Greaves, The rare earth elements in seawater. Nature, 296, 214, 1982.https://doi.org/10.1038/296214a0
[37] D. Z. Piper, Rare earth elements in the sedimentary cycle: A summary. Chemical geology, 14 (4), 285-304, 1974. https://doi.org/10.1016/0009-2541(74)90066-7.
[38] C. R. German and H. Elderfield, Rare earth elements in Saanich Inlet, British Columbia, a seasonally anoxic basin. Geochimica et Cosmochimica Acta, 53 (10), 2561-2571, 1989. https://doi.org/10.1016/0016-7037(89)90128-2.
[39] W. G. Powell, P. A. Johnston and C. J. Collom, Geochemical evidence for oxygenated bottom waters during deposition of fossiliferous strata of the Burgess Shale Formation. Palaeogeography, Palaeoclimatology, Palaeoecology, 201 (3), 249-268, 2003. https://doi.org/10.1016/S0031-0182(03)00612-6.
[40] S. M. McLennan, S. Hemming, D. K. McDaniel and G. N. Hanson, Geochemical approaches to sedimentation, provenance and tectonics. In M. J. Johnsson, A. Basu (Eds.), Geological Society of America Special Papers, Processes Controlling the Composition of Clastic Sediments, pp. 21-40, 1993.
[41] W. R. Dickinson and C. A. Suczek, Plate tectonics and sandstone compositions. AAPG Bulletin, 63 (12), 2164-2182, 1979.

[42] S. Critelli, P. E. Rumelhart and R. V. Ingersoll, Petrofacies and Provenance of the Puente Formation (Middle to Upper Miocene), Los-Angeles Basin, Southern California - Implications for Rapid Uplift and Accumulation Rates. Journal of Sedimentary Research Section a-Sedimentary Petrology and Processes, 65 (4), 656-667, 1995.

[43] H. Dokuz, Çankırı-Çorum Havzası Oligosen kumtaşlarının petrografisi ve provenansı, Yozgat. Ömer Halisdemir Üniversitesi Mühendislik Bilimleri Dergisi, 7 (3), 1089-1094, 2018. https://doi.org/10.28948/ngumuh.502251

[44] K. Hayashi, H. Fujisawa, H. D. Holland and H. Ohmoto, Geochemistry of similar to 1.9 Ga sedimentary rocks from northeastern Labrador, Canada. Geochimica et Cosmochimica Acta, 61 (19), 4115-4137, 1997. https://doi.org/10.1016/S0016-7037(97)00214-7.

[45] L. Zhou, Z. Wang, W. Gao, K. Zhang, H. Li and L. Zhang, Provenance and tectonic setting of the Lower Cambrian Niutitang formation shales in the Yangtze platform, South China: Implications for depositional setting of shales. Geochemistry, 79 (2), 384-398, 2019. https://doi.org/10.1016/j.chemer.2019.05.001.

[46] R. L. Cullers, Implications of elemental concentrations for provenance, redox conditions, and metamorphic studies of shales and limestones near Pueblo, CO, USA. Chemical geology, 191 (4), 305-327, 2002. http://dx.doi.org/10.1016/S0009-2541(02)00133-X.

[47] B. P. Roser and R. J. Korsch, Provenance signatures of sandstone-mudstone suites determined using discriminant function analysis of major-element data. Chemical geology, 67 (1–2), 119-139, 1988. http://dx.doi.org/10.1016/0009-2541(88)90010-1.

[48] P. A. Floyd and B. E. Leveridge, Tectonic environment of the Devonian Gramscatho basin, south Cornwall: Framework mode and geochemical evidence from turbiditic sandstones. Journal of the Geological Society, 144, 531-542, 1987. https://doi.org/10.1144/gsjgs.144.4.0531

[49] D. Bal Akkoca and Z. Baytaşoğlu, The mineralogy and geochemistry of Neogene sediments from eastern Turkey, southeast of Arapgir (Malatya). Turkish Journal of Earth Sciences, 22 (4), 645-663, 2013. https://doi.org/10.3906/yer-1202-13

[50] D. J. Wronkiewicz and K. C. Condie, Geochemistry and provenance of sediments from the Pongola Supergroup, South Africa: Evidence for a 3.0-Ga-old continental craton. Geochimica et Cosmochimica Acta, 53 (7), 1537-1549, 1989. http://dx.doi.org/10.1016/0016-7037(89)90236-6.

[51] J. S. Armstrong-Altrin, Y. I. Lee, S. P. Verma and S. Ramasamy, Geochemistry of Sandstones from the Upper Miocene Kudankulam Formation, Southern India: Implications for Provenance, Weathering, and Tectonic Setting. Journal of Sedimentary Research, 74 (2), 285-297, 2004. https://doi.org/10.1306/082803740285.

[52] L. Sun, H. Gui and S. Chen, Geochemistry of sandstones from the Neoproterozoic Shijia Formation, northern Anhui Province, China: Implications for provenance, weathering and tectonic setting. Chemie der Erde - Geochemistry, 72 (3), 253-260, 2012. https://doi.org/10.1016/j.chemer.2011.11.006.

[53] Z. W. Wang, J. Wang, X. G. Fu, W. Z. Zhan, J. S. Armstrong-Altrin, F. Yu, X. L. Feng, C. Y. Song and S. Q. Zeng, Geochemistry of the Upper Triassic black mudstones in the Qiangtang Basin, Tibet: Implications for paleoenvironment, provenance, and tectonic setting. Journal of Asian Earth Sciences, 160, 118-135, 2018. https://doi.org/10.1016/j.jseaes.2018.04.022.

[54] R. L. Cullers and J. L. Graf, Rare earth elements in igneous rocks of the continental crust: predominantly basic and ultrabasic rocks. In Rare earth element geochemistry, pp. 237-274, Elsevier Amsterdam, 1984.

[55] S. R. Taylor and S. M. McLennan, Chemical composition and element distribution in the Earth's crust. In R. A. Meyers (Ed.), Encyclopedia of Physical Science and Technology (Third Edition), pp. 697-719, Academic Press, New York, 2003.

[56] R. L. Cullers and V. N. Podkovyrov, The source and origin of terrigenous sedimentary rocks in the Mesoproterozoic Ui group, southeastern Russia. Precambrian Research, 117 (3–4), 157-183, 2002. http://dx.doi.org/10.1016/S0301-9268(02)00079-7.

[57] K. C. Condie, Chemical composition and evolution of the upper continental crust : Contrasting results from surface samples and shales. Chemical geology, 104, 1-37, 1993.

[58] R. L. Cullers, The geochemistry of shales, siltstones and sandstones of Pennsylvanian-Permian age, Colorado, USA: implications for provenance and metamorphic studies. Lithos, 51 (3), 181-203, 2000. http://dx.doi.org/10.1016/S0024-4937(99)00063-8.

[59] S. M. McLennan, S. R. Taylor, M. T. McCulloch and J. B. Maynard, Geochemical and Nd-Sr isotopic composition of deep-sea turbidites: Crustal evolution and plate tectonic associations. Geochimica et Cosmochimica Acta, 54 (7), 2015-2050, 1990. http://dx.doi.org/10.1016/0016-7037(90)90269-Q.

[60] R. L. Cullers, The controls on the major- and trace-element evolution of shales, siltstones and sandstones of Ordovician to tertiary age in the Wet Mountains region, Colorado, U.S.A. Chemical geology, 123 (1–4), 107-131, 1995. http://dx.doi.org/10.1016/0009-2541(95)00050-V.

[61] R. L. Cullers, A. Basu and L. J. Suttner, Geochemical signature of provenance in sand-size material in soils and stream sediments near the Tobacco Root batholith, Montana, U.S.A. Chemical geology, 70 (4), 335-348, 1988. http://dx.doi.org/10.1016/0009-2541(88)90123-4.

[62] M. M. Karadağ, Geochemistry, provenance and tectonic setting of the Late Cambrian–Early Ordovician Seydişehir Formation in the Çaltepe and Fele areas, SE Turkey. Geochemistry, 74 (2), 205-224, 2014. https://doi.org/10.1016/j.chemer.2013.07.002.

[63] D. Boztuğ and Y. Harlavan, K–Ar ages of granitoids unravel the stages of Neo-Tethyan convergence in the eastern Pontides and central Anatolia, Turkey. International Journal of Earth Sciences, 97 (3), 585-599, 2008. https://doi.org/10.1007/s00531-007-0176-0.

[64] D. Boztuğ, R. C. Jonckheere, M. Heizler, L. Ratschbacher, Y. Harlavan and M. Tichomirova, Timing of post-obduction granitoids from intrusion through cooling to exhumation in central Anatolia, Turkey. Tectonophysics, 473 (1), 223-233, 2009. https://doi.org/10.1016/j.tecto.2008.05.035.

[65] S. Köksal, R. L. Romer, M. C. Göncüoglu and F. Toksoy-Köksal, Timing of post-collisional H-type to A-type granitic magmatism: U–Pb titanite ages from the Alpine central Anatolian granitoids (Turkey). International Journal of Earth Sciences, 93 (6), 974-989, 2004. https://doi.org/10.1007/s00531-004-0432-5.

[66] İ. Kuşcu, G. Gençalioğlu Kuşcu, L. D. Meinert and P. A. Floyd, Tectonic setting and petrogenesis of the Çelebi granitoid, (Kırıkkale-Turkey) and comparison with world skarn granitoids. Journal of Geochemical Exploration, 76 (3), 175-194, 2002. https://doi.org/10.1016/S0375-6742(02)00254-6.

[67] K. Koçak, Mineralogy, geochemistry, and Sr–Nd isotopes of the Cretaceous leucogranite from Karamadazı (Kayseri), central Turkey: implications for their sources and geological setting. Canadian Journal of Earth Sciences, 45 (8), 949-968, 2008. https://doi.org/10.1139/E08-040

[68] J. S. Armstrong-Altrin, Evaluation of two multidimensional discrimination diagrams from beach and deep-sea sediments from the Gulf of Mexico and their application to Precambrian clastic sedimentary rocks. International Geology Review, 57 (11-12), 1446-1461, 2015. https://doi.org/10.1080/00206814.2014.936055

[69] Q. Du, Z. Han, X. Shen, C. Han, Z. Song, L. Gao, M. Han and W. Zhong, Geochronology and geochemistry of Permo-Triassic sandstones in eastern Jilin Province (NE China): Implications for final closure of the Paleo-Asian Ocean. Geoscience Frontiers, 10 (2), 683-704, 2019. https://doi.org/10.1016/j.gsf.2018.03.014.

[70] M. R. Bhatia, Plate tectonics and geochemical composition of sandstones. The Journal of geology, 91 (6), 611-627, 1983.

[71] B. P. Roser and R. J. Korsch, Determination of tectonic setting of sandstone - mudstone suits using SiO2 content and K2O/Na2O ratio. Journal of Geology, 94, 635-650, 1986. citeulike-article-id:5332564.

[72] M. R. Bhatia and K. A. W. Crook, Trace element characteristics of graywackes and tectonic setting discrimination of sedimentary basins. Contributions to Mineralogy and Petrology, 92 (2), 181-193, 1986. https://doi.org/10.1007/BF00375292

[73] S. P. Verma and J. S. Armstrong-Altrin, Geochemical discrimination of siliciclastic sediments from active and passive margin settings. Sedimentary Geology, 332, 1-12, 2016. https://doi.org/10.1016/j.sedgeo.2015.11.011

[74] T. A. LaMaskin, R. J. Dorsey and J. D. Vervoort, Tectonic controls on mudrock geochemisry, Mesozoic rocks of eastern Oregon and western Idaho, USA: Implications for cordilleran tectonics. Journal of Sedimentary Research, 78 (12), 765-783, 2008.